LAUNCH SOUND LEVEL CHARACTERISATION AND MITIGATION: NUMERICAL MODELLING FRAMEWORK AND METAMATERIAL PROOF OF CONCEPT.

M.S. Escartí-Guillem[1,6], J.M. Requena-Plens[2], P. Barriuso Feijoo[1], A. Cebrecos[3], M. Chimeno Manguán[4], P. Cobo Parra[5], L.M. García-Raffi[6], J.-P. Groby[7], S. Hoyas[6], N. Jiménez[3], M. Lázaro[6], J. Leng[7], J. Nieto Mocholí[1], E. Roibás Millán[4], V. Romero-García[7], R. Picó [2], V. Sánchez-Morcillo[2], F. Simón Hidalgo[8], and I. C.S. Ngan[9]

[1]*Comet Ingeniería, Convento Carmelitas, 2, 46010 Valencia (Spain), mescarti@comet-ingenieria.es, pbarriuso@comet-ingenieria.es, jnieto@comet-ingenieria.es*

[2]*Universitat Politècnica de València, C/ Paranimf, 1, 46730 Grau de Gandía (Spain), jmreplens@gmail.com, rpico@fis.upv.es, victorsm@fis.upv.es*

[3]*Instituto de Instrumentación para Imagen Molecular, CSIC-UPV, CAMINO DE VERA s/n, 46022 València, Spain, alcebrui@i3m.upv.es, nojigon@i3m.upv.es*

[4]*Universidad Politécnica de Madrid, Pza. Cardenal Cisneros, 3, 28040 Madrid (Spain), marcos.chimeno@upm.es, elena.roibas@upm.es*

[5]*ITEFI-CSIC, C/ Serrano 144, 28006 Madrid (Spain), pedro.cobo@csic.es*

[6]*Instituto Universitario de Matemática Pura y Aplicada UPV, Camino de Vera s/n, 46022 Valencia (Spain), maesgui2@etsid.upv.es, lmgarcia@mat.upv.es, serhocal@upvnet.upv.es, malana@mes.upv.es*

[7]*Laboratoire d'Acoustique de l'Université du Mans (LAUM), UMR-CNRS 6613 - Le Mans Université, Avenue O. Messiaen, 72085 Le Mans Cedex 9 (France), jpgroby@univ-lemans.fr, julien.leng.etu@univ-lemans.fr, vicente.romero@univ-lemans.fr*

[8]*ITEFI-CSIC, C/ Serrano 144, 28006 Madrid (Spain), f.simon@csic.es*

[9]*ESA/ESTEC, Keplerlaan 1, PO Box 299, 220AG Noordwjijk (The Netherlands), ivan.ngan@esa.int*

ABSTRACT

Due to the severe acoustic environment during space vehicle lift off the prediction and mitigation of acoustic levels becomes a vital issue. This paper conforms the engineering background needed to develop a new sound mitigation method for vehicle launchers. The sound propagation within a launch event has been analysed with dedicated CFD, identifying the shock waves and the evolution of the SPL generated. Data analysis of the pressure field surrounding the fairing demonstrates a vertical directivity. On the structural domain, a numerical modelling framework composed of an hybrid FEM/BEM/SEA model has been postulated. The results provide the basis to analyse the mitigation structures proposed. On the acoustic side, two different metamaterial structures are presented, both made of a periodic unit cell of Helmholtz resonators. On the launch pad, the metamaterial partially covers the exhaust channels and provides quasi-perfect broadband sound absorption. On the fairing the metamaterial is added to the existing wall and introduce an absorption peak. These findings provide a noise mitigation technique that has the potential to improve the attenuation efficiency, thus, reducing the acoustic loading and the risk of technical failure during the launch stage.

Key words: Launch noise, Vibro-acoustic, CFD, Metamaterial.

1. INTRODUCTION

The actual acoustic conditions during the launch of space vehicles are extremely complex, with intense pressure levels, temperatures and flows. The jet of exhaust gases from the rocket engine and its impact with the launch facility generates severe acoustic waves, which are the main sound sources during the lift off stage [1, 2]. This acoustic environment causes a severe acoustic and vibrating loading on the payload which threatens the entire mission leading to potential economic losses [3]. Hence, the prediction and mitigation of the acoustic levels during the lift off stage play an important role in the design process of the launch complex and the space vehicle since it improves the reliability of the launchers and at the same time the comfort of the payloads.

In this work, carried out under a programme of the European Space Agency, we propose and design a sound mitigation method applicable to an actual launch configuration. The goal is to obtain a significant decrease of the sound pressure levels generated during the lift-off of a Vega rocket and a reduction of the acoustic loads experienced by the payload inside the fairing. Furthermore, to study the application of acoustic noise reduction solutions for the VEGA fairing and other ESA future launch vehicles a numerical modelling framework is needed.

The precise knowledge of the acoustic levels, and the vibro-acoustic dynamic response becomes a big chal-

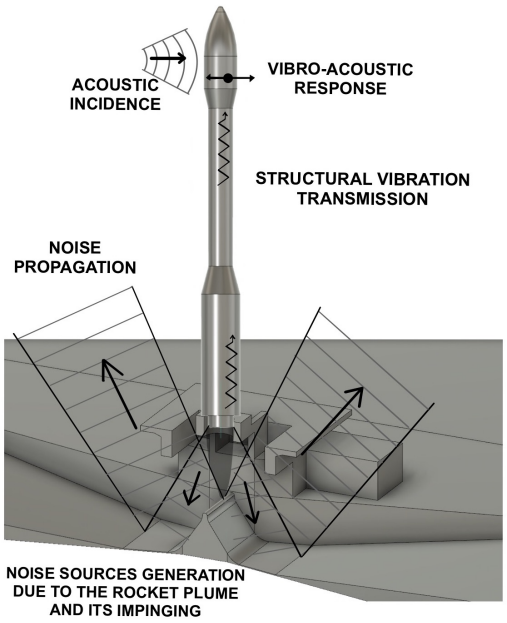


Figure 1: Sound generation and transmission paths at rocket launch.

lenge due to the complexity of the problem. The global study of the sound generation and transmission up to the payload implies several problems of different nature. The first step is to identify the noise sources, which involves the resolution of an aero-acoustic problem that includes the study of the engine exhaust jet and its interference with the launch platform. Second, an acoustic study is required to model the propagation and incidence of the free-field airborne noise on the structure. At last, the resolution of a vibro-acoustic problem is needed: a structural transmission of loads is found from the rocket structure to the payload and the fairing. So that the structural vibration of the fairing interacts with the acoustic pressure field of the air inside the fairing.

The proposed approach is to address the mitigation of the acoustic levels with two different solutions. On one hand, a solution is intended to be implemented on the launch pad exhaust channels to strongly reduce the reflected acoustic wave generated by the engine exhaust gases. On the other hand, a layer of metamaterial is added to the existing honeycomb structure of the fairing to reduce the acoustic loads reaching the payload. The metamaterial consists of panels made of periodic distributions of waveguides loaded by Helmholtz resonators. The resonances of each resonator introduce a strong dispersion around its resonance frequency that will affect the resonance frequency of the global system. The result is a wavelength of the working frequency much bigger than the system. This provides properties to the structure not available in traditional materials with reduced dimensions [4]. However, for this kind of systems the real challenge is to obtain both subwavelength and perfect absorption [5]. Perfect absorption is accomplished when the energy leakage and the inherent losses of the system are perfectly balanced. We accomplish this condition tuning the losses with a proper design of the geometry of the resonators [6]. This kind of structures have been extensively analysed during the last years to develop perfect acoustic absorbers in the low frequency range.

The work is organised as follows. In Section 2 we define the problem analysed in this work. The modelling framework is presented in Section 3. In Section 4 we present the two metamaterial configurations design to reduce the sound pressure level. Section 5 summarises the conclusions of the work.

2. DEFINITION OF THE PROBLEM

High sound pressure levels at the launch pad are not dangerous by itself because launch pads are sufficiently robust to support such levels [3]. However, it is the interaction of the ambient sound with the exterior surface of the vehicle, and the resulting acoustically-induced vibration of the vehicle that should be maintained below safe levels. Eldred [1] stated that the maximum reduction in acoustic loading to be sought is on the order of 15 to 20 dB. Any further suppression would not be meaningful since the vehicle would encounter a higher level of noise during flight.

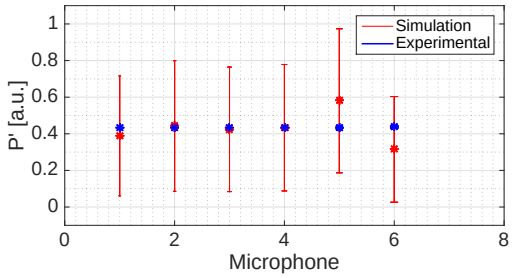
The liftoff phase induces acoustic loads in the launch vehicle over a broad frequency range [1, 7]. This noise comes mainly from the jet, who creates three different sound sources [2, 8]: turbulent mixing noise, impinging tones, and shock noise. The first noise source is the one generated by the turbulent mixing at the mixing layer. This noise can be due to the large-scale or small-scale eddies. However, at supersonic conditions the noise produced by the big scale vortexes is prevalent and creates low frequency noise with a high directivity downstream [9]. The second noise source are the screech tones produced by the shock waves that appear because of the pressure difference. In contrast to the large-scale turbulent mixing noise, the screech tones are broadband and are directed primarily upstream where the launch vehicle would be located [2]. Finally, the impinging tones appear when the impact of the jet takes place and just as the broadband noise, it is directed upstream [2]. However, the screech tones diminish their influence when the jet impacts the deflector. This noise sources interact with the launch platform and induce strong acoustic loads on the launch structures and the space vehicle. The noise mitigation can be achieved by methods which can be classified as those acting outside the vehicle, at the launch pad level, or inside it to protect the fairing from vibrations induced by the acoustic load.

The main strategies to decrease the sound pressure levels at the launch pad environment are the following: to increase sound absorption (which is very low in common air atmosphere), to avoid direct ground reflections towards the vehicle by proper launch pad design or to de-

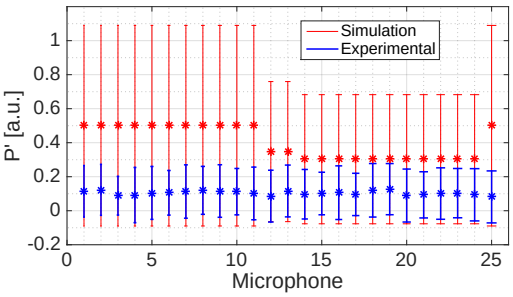
crease the noise emitted by the source. The last option implies the selection of less-noisy rocket engines, which will not normally be possible since engine selection is determined by other requirements. The most extended method to reduce the noise pressure level by sound absorption is the injection of water at given locations around the pad. Water mitigates all the three components of jet noise [10]. When the water is injected into the exhaust plume this is dispersed faster so the far-field noise is reduced [11]. Different studies demonstrate that water deluge and water injection are efficient methods for noise reduction, and average values of noise reduction are around 10 dB when acting on isolated sources, and around 5 dB when sources interact with the launch pad. A significant disadvantage of this technique is that water can degrade materials and structures [7], and adversely affects the diffuser performance [11]. Regarding the design of the launch pad, it usually includes sub-surface channels and flame deflectors whose design is mostly oriented to act on exhaust gases at the ignition and initial lift-off stages [12]. The channel walls and bottom, mainly made up of refractory concrete, are efficient reflectors of sound waves, and therefore far to be optimal from the noise management point of view. Research in this area [7, 13, 14] indicates that factors such as trench cover and shape have a significant effect on its ability to reduce noise, and that there are two main types of acoustic sources associated with flame deflectors [14]: impinging noise and mach wave radiation. Finally, a new direction of research was recently proposed, based on the use of sonic crystals, covering the channels to enhance the scattering of the acoustic fields into different directions (non-specular reflections) [12]. By comparison with a reference flat reflector, it was observed that reflected waves spread in space as a consequence of the spatially modulated properties of the crystal. Due to this spreading the system produces a broadband noise reduction in the area of the source.

Regarding the noise control in the fairing, the objective is to reduce sound levels to prevent harmful effects on the payload. Sound absorbing materials are used to increase the transmission loss across multilayer walls, to decrease the reverberation in enclosures, or to attenuate noise produced by internal sources. The combined use of insulating/absorbing materials allows designing lighter sandwich structures for attenuating noise incoming from outside sources. Traditional means of acoustic absorption make use of porous or fibrous materials [15], gradient index materials, or perforated or micro-perforated panels (MPPs) [16, 17], in front of an optimised depth cavity. The absorption band can be extended by designing multiple-layer MPPs (ML-MPP) containing MPP and air cavities only [18, 19, 20], or combining these with porous layers [21, 22, 23].

The proposed solution is based on removing the acoustic field coming into the fairing in two stages. First, some noise is reduced through the propagation path at the launch pad, so the spectrum to be expected at the fairing could be modified. Second, the noise getting into the fairing is reduced by increasing the transmission loss of the fairing shell.



(2.a) Faring microphones



(2.b) Mast microphones

Figure 2: Time averaged pressure validation against experimental measurements. Results are normalised.

3. SOUND LEVEL CHARACTERISATION

The first step towards the evaluation of any mitigation process is an identification of the sources responsible for noise generation. Making use of experimental data from a Vega Launch, the different phenomena produced during the lift-off phase have been studied. Data collected by microphones at an antenna provide insight into rocket noise sources. Inside the fairing the spectrum profile has a maximum located around 400 Hz. Outside the fairing the range with high values extends from 200 Hz to 1 kHz.

3.1. Computational Fluid Dynamics

Until about twenty-five years ago the prediction methods for aircraft noise were mainly semi- empirical, and were based on the laws established by Lighthill [24]. Today, measurement on the real scale is limited by the intrinsic difficulty of obtaining such data in such a hostile environment with very intense pressure and temperature levels [2]. Computational fluid dynamics, CFD, has the potential to replace the empirical experiments because it allows the collection of information regarding the phenomena that occur at launch, both spatially and temporally. Thus facilitating the comprehension of the generation and propagation mechanisms of noise.

Our objective is to compute almost all the launch environment. This modelling approach can be used to check any characteristics of the flow. The geometry included in the model consists of the VEGA rocket, the launcher support system, the flame deflector, the exhaust ducts and the

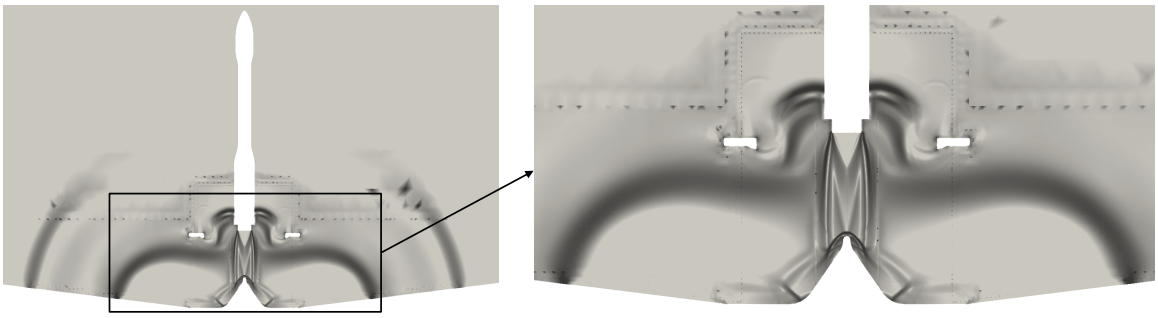


Figure 3: Synthetic representations of Schlieren images in order to visualise the shock waves.

floor. The tool used for the aero-acoustic simulations is the software OpenFOAM v6. The turbulence model used is an Unsteady RANS simulation with a kOmegaSST model. The acoustic field that the launch vehicle must withstand is largely due to the fluctuating component of the turbulence of the engine's exhaust gas jet mixture layer. In the RANS turbulence model all scales of turbulence are modelled and the information about the variables counted does not provide the fluctuating part but only the mean component. This is a limitation of the work because the component of the noise due to the fluctuating pressure can not be detected. However, the transient nature of the model allows the collection of information on pressure variations due to shock waves and the average of turbulence. Moreover, as the objective was to assess the noise source regions, we have focused on the region where the rocket jet plume develops and where it impacts with the deflector. We generated a mesh with 10M elements and a cell size of 0.39 mm in the jet region. All the details regarding the simulation can be found on [25].

No data was readily available for the validation of the CFD simulations at the near region of the exhaust gases. However, experimental data placed at the far field and in the fairing has been provided. Therefore, this data is used to assess the error of the CFD approach. The first set of experimental data has been extracted from a phased array of microphones located at one of the masts surrounding the launch platform. The second set consists of the measurements of six microphones along the faring. In Figure 2 we compare the time average value of the total pressure at each microphone with the equivalent positions translated to the simulations. The blue line represents the acceptable range extracted from the experimental measures, calculated as the mean value ± the standard error. The red line represents the range covered by the deviation of the simulation results. Regarding the mast microphone data, none of the microphones mean pressure obtained by the simulation is inside the experimental acceptable range. However, the experimental acceptable range is inside the mean minus the standard error of the simulation. The comparison at the fairing shows that at microphones 2, 3 and 4 the mean pressure obtained from the CFD model is inside the acceptable range while none of the others is. The performance of the CFD model is not ideal in this region. For both locations, there are factors as the simplifications of the exhaust plume input data or the movement of the rocket which lead into different sources of error. However, the parameters obtained at the plume development region and the behaviour of the flow coincide with what can be found on the literature. Therefore, we believe that the CFD results at the near plume region are satisfactory.

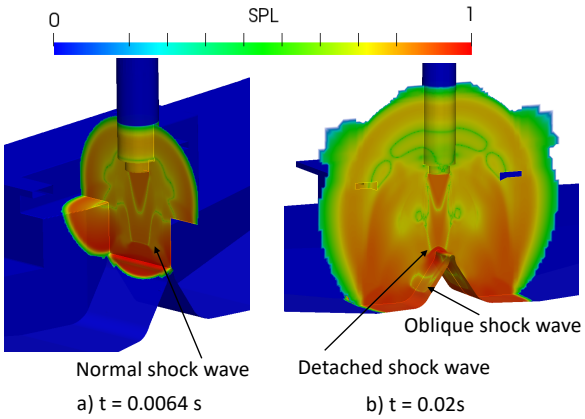


Figure 4: Normalised Sound Pressure Level contour of Vega launch pad environment

Experimentally noise generation areas due to shock waves can be visualised with Schlieren images which capture the density variations of the fluid. Figure 3 shows a synthetic version of the Schlieren images. The first big density change happens in the boundary of the moving flow. In the jet region, there is a density variation due to the boundary of the jet core. In addition, different oblique shock waves appear which join towards the centre of the axis until they converge at the detached wave over the deflector. The next variation observed is two twin oblique shock waves formed just on the curve preceding the ramp on each side of the deflector. Thereby, the main shock waves observed are those due to the jet and the moving flow on the platform, the detached wave on the deflector and the oblique shock wave in the change of curvature of the ramp. In this way, all these disturbances are noise generating sources.

Once the location of the shock waves is identified, the sound pressure level (SPL) has been represented to vi-

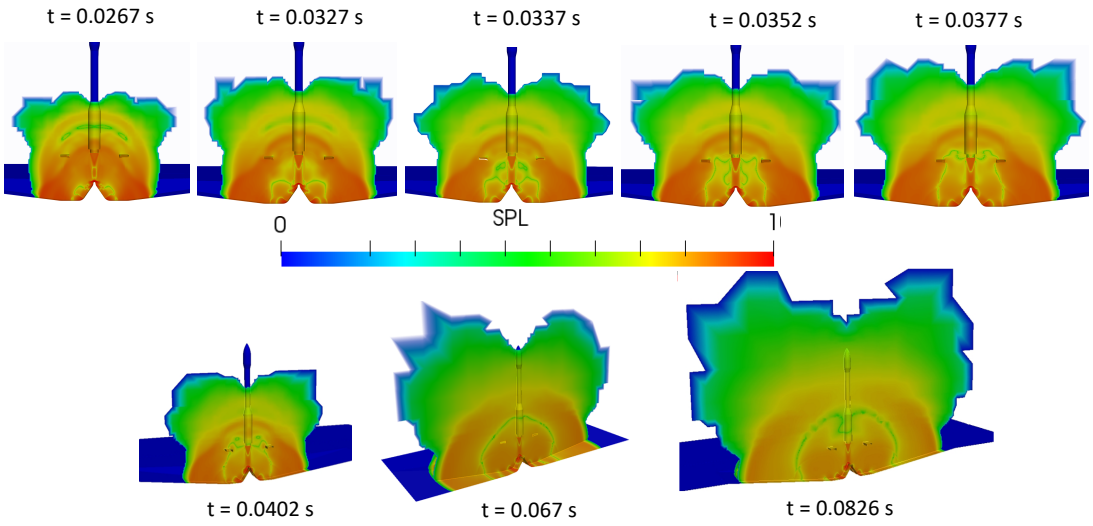


Figure 5: Normalised Sound Pressure Level (SPL) contour of Vega launch pad environment

sualise the regions where the sound pressure intensity is higher. As the jet flow is supersonic there is a normal shock wave whose SPL originated is close to maximum dB as can be seen on the Figure 4 a). As the flow propagates this wave is deformed due to the presence of the deflector resulting in the detached shock wave already seen on the Schlieren images. At this instant presented on Figure 4 b), the maximum SPL levels appear caused by the impact of the normal shock wave with the tip of the deflector. Later, the wave front will stay at the curvature between the deflector and the floor because at that point there is located an oblique shock wave. Moreover, there is a green wave front that corresponds with the jet core boundary and a second one that emerges from the nozzle and moves downstream being disturbed by the elements of the launch pad. The evolution of this second wave front can be seen on the top pictures of Figure 5, between 0.0267 s and 0.0377 s. It is originated by the initial exit of the gases and its impact with the deflector. As it propagates upstream it gets disturbed by the elements of the structure. Later as seen on the lower pictures of Figure 5, the fluid front continues to advance upstream, while the waves due to the interaction with the support structure, begin to separate from the wave that continues to be generated at the output of the jet. It has to be noted that due to the higher speed of sound propagation, the wave front overtakes the fluid front and is finally attenuated as can be seen on the last instant of time. On this basis, we can conclude that the maximum SPL is produced by the normal shock wave that appears at the beginning and its subsequent impact with the deflector. This impact, combined with the effect of the movement of the flow, causes the acoustic waves to propagate upstream of the vehicle.

In a diffuse sound field, the time average of the mean square sound pressure is everywhere the same and the flow of acoustic energy in all directions is equally probable. The analysis of the spatial dispersion of the experimental results on the exterior of the fairing showed that the pressure is almost the same at all the microphones, therefore this approach has been considered in the vibroacoustic analysis showed in Section 3.2. However, only information regarding 6 locations at the exterior of the fairing was available. This seems a limited amount of information. Hence, the diffuse acoustic field hypothesis is studied taking advantage of the CFD results.

A total of 176 sampling points surrounding the fairing have been computed to evaluate the pressure field. These points are separated in 11 axial planes with 16 equally spaced points. Figure 6 shows, at the left part, the results obtained for a set of points placed in the same azimuth angle but at different height and, at the central and right part, the results for two sets at the same height but in different azimuth angles. The gauge pressure increases as the wave front due to the exhaust gases moves upstream. After reaching the maximum the gauge pressure decreases as a result of the second wave front. It can be seen how for the different height planes the gauge pressure is delayed on time. Moreover, the maximum of the peak pressure decreases with height so the pressure wave reduces its magnitude as it propagates. Concerning the sound pressure level, SPL, there is no mismatch between points at different revolution angles. The discrepancy of both pressure and SPL between points at the same height is small. But there is an increase of this difference with the increase of height. The maximum variation of pressure between points at the same plane is about 1/10 of that for the points at different heights. Moreover, the difference of SPL at different heights is 10.6 db while at the same plane is 0.32 dB for case b) and 1.25 dB for case c). This is mainly because the fluid front reaches each plane at a different time. Also, it should be noted that the region at the lower part of the fairing supports bigger pressure values than the upper region.

Besides, to assess the directivity of pressure waves the pressure gradient can be analysed. As the pressure wave moves upwards the pressure gradient on the rocket changes over time. Figure 7 shows the evolution of the

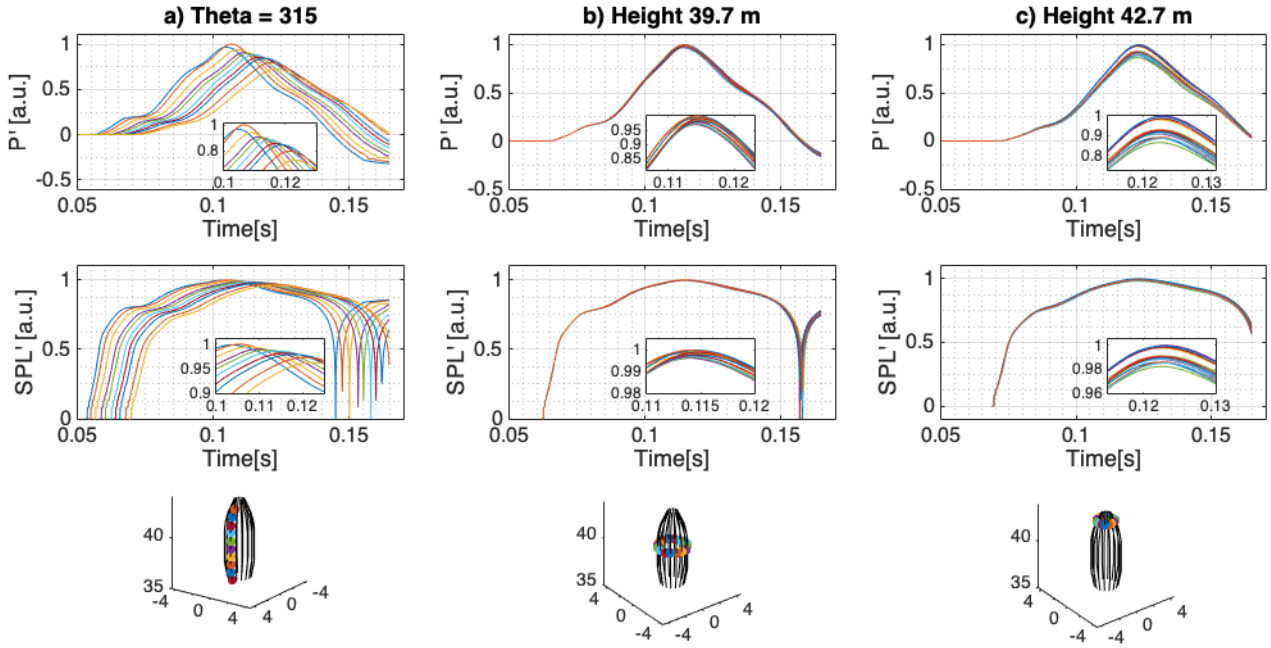


Figure 6: Normalised pressure and normalised SPL at different heights (a) and at different azimuth angles (b and c).

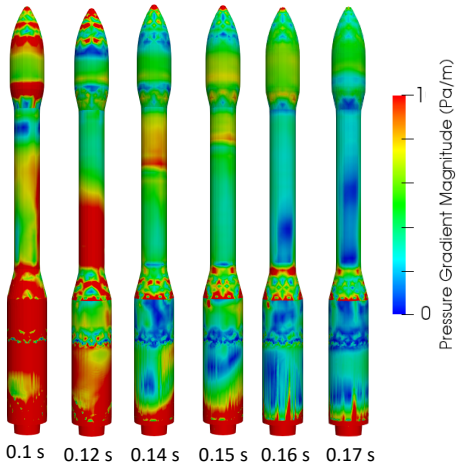


Figure 7: Temporal evolution of normalised pressure gradient magnitude along the VEGA rocket.

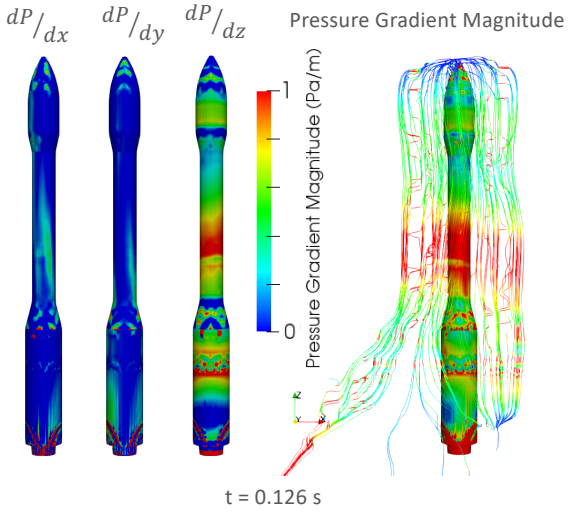


Figure 8: Pressure gradient components and magnitude.

magnitude of the pressure gradient over the rocket between the instant 0.1 s and 0.17 s. At the first instant of time, the maximum pressure gradients are at the bottom of the rocket and at the middle of the second stage of the rocket due to the action of the high-speed gases. While the exhaust gases propagate, the intensity of the pressure gradient moves upwards. As a results of the propagation of the pressure field the intensity of the pressure gradient decreases with time until the last instant where the pressure gradient has its lowest value. Therefore, the pressure gradient values at the payload fairing are also reduced with time.

The pressure gradient magnitude is composed by the gradient at each of the main directions. Figure 8 shows the pressure gradient at each directions and the magnitude along with the streamlines of the pressure gradient. It is clear that the pressure gradient at the X and Y coordinates are lower than the one at the axial direction. The streamlines show that the pressure gradient moves along the axial direction and converge at the tip of the payload faring. At the tip, the main contributor is the Z negative component. This negative component creates a gradient pressure force that attracts the flow. In conclusion, the component Z is the main contributor to the gradient of pressure. This gradient diminish as the pressure wave is attenuated and the maximum values happen around the instant of time 0.1 s.

3.2. Vibro-acoustic response

The development of numerical models has been carried out to model the vibro-acoustic behaviour of a VEGA launcher during the lift-off. The goal is to provide a numerical simulation framework for the posterior analysis of acoustic reduction solutions proposed in this work. Due to the high complexity of manufacturing and testing a 1:1 fairing mock-up, a reliable numerical model for the VEGA fairing is required.

No other elements apart from the fairing itself are considered in the model. Therefore, the model consists of an exterior acoustic unbounded domain, the fairing as the structural domain and a second acoustic domain which represents the air inside the fairing. The relevant frequency bands regarding the current acoustic load inside the fairing are between 200 Hz and 1250 Hz in terms of third octave bands. Given the characteristics of the system under study it is not appropriate to develop and solve a single numerical model for the whole frequency range. Therefore, an approach based on multiple numerical models for multiple frequency ranges is adopted. The modelling approach for the low frequency range is based on a BEM-FEM-BEM model for the external air, the fairing structure and the internal air respectively. In the high frequency range, the Statistical Energy Analysis (SEA) is selected as recommended by the ECSS [26]. In addition, the SEA formulation combined with the low frequency selected methods results in an efficient hybrid model for the medium frequency range. Hence, the medium frequency range is analysed through the Shorter and Langley method [27] for the interaction between FEM and SEA. In order to define the different frequency ranges involving different numerical methods, the applicability frequency range of SEA is established at 630 Hz band. This frequency threshold is limited by a minimum mode count of 6 resonant modes per 1/3 octave band [28]. This modelling technique is available in VA One simulation software, by ESI group [29], that has been used for obtaining the simulation results shown in this paper.

The fairing structure is considered to be compound of three different structural elements given their different geometry: the bottom section or boat-tail, the cylindrical section and the concave end, ogive. In addition, the payload adapter (PLA) has been included in the study. The fairing external structure is assumed to be composed of 2 mm thick M55J skins and an aluminium honeycomb core, with density 49.66 $\mathrm{kg/cm^3}$. For the low frequency model, the FEM mesh size has been determined to provide 6 elements per wavelength up to 1000 Hz, resulting in a mean mesh size of 0.04 m. The SEA model is based on a SEA sandwich plate with analogous properties. As there was not information available regarding the fairing structural damping, a damping law against frequency has been defined. In order to provide a reasonable damping value for the sandwich structure alone, a constant loss factor of 1 % is considered for the low frequency model and a decay as $\eta \propto f^{1/2}$ for the high frequency model. For the external fluid a null loss factor is considered while

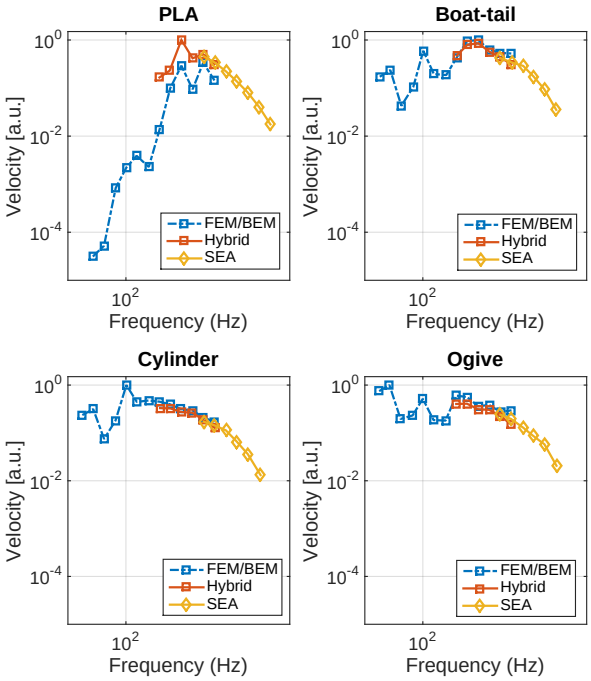
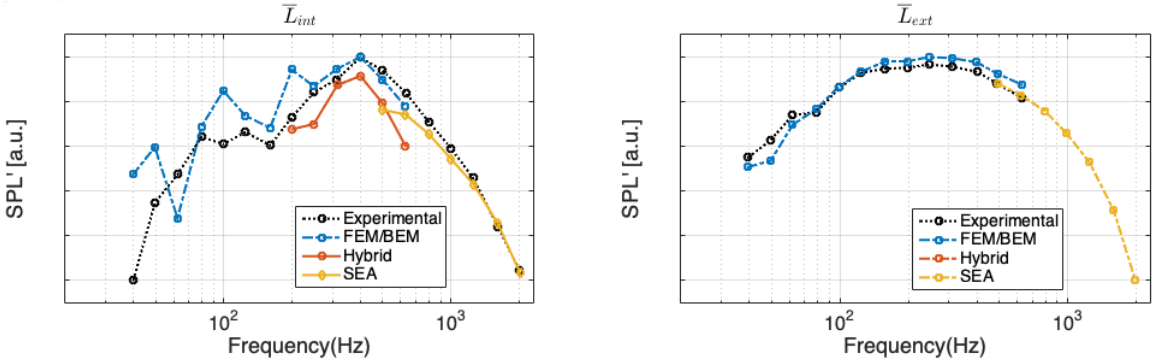


Figure 9: Structural response in 1/3-octave bands. Normalised velocity.

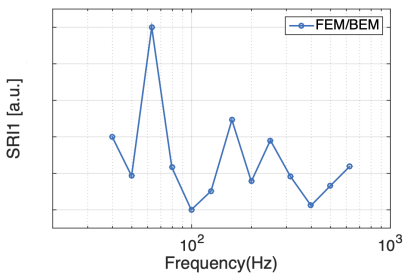
for the internal air, due to the presence of auxiliary elements and the possible surfaces finishes a variable loss factor is used. The acoustic load acting on the fairing is assumed to be a diffuse acoustic field.

The structural response of the fairing has interest as an indicator of the dynamics of the whole system, to assess the continuity between models applicable in different frequency ranges. In the low frequency model the structural response is calculated only at five locations per structural element due to very high computation cost. In the hybrid and high frequency models, in addition to these, the spatial average velocity per component has been calculated. The comparison between the three magnitudes is shown in Figure 9. Good agreement is found for all the elements except for PLA, that shows the largest differences between the low frequency model and the rest of the results. The good agreement between the single point velocity and the spatial mean of the hybrid models shows that the point velocity of the low frequency model is a good estimator of the global response at least at the frequency bands compared.

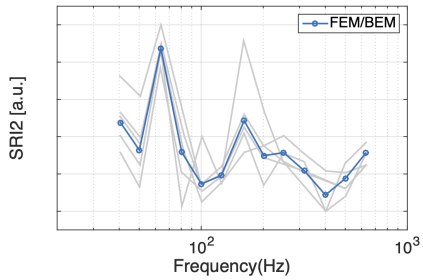
To overcome the limited information to model the vibro-acoustic behaviour of the launcher, an adaptation term between the model developed and the available experimental data from the Vega lift-off has been defined. A linear relationship has been assumed between the quadratic acoustic pressure measured during the launching and the one obtained by the model. If the acoustic pressure is expressed in level scale the adaptation term C can be obtained subtracting the sound pressure levels correspond-



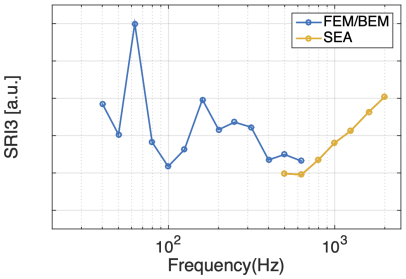
(10.a) Comparison between measurements and numerical normalised SPL inside (left) and outside (right) the fairing.



(10.b) SRI1 in 1/3-octave bands through the low frequency model.



(10.c) SRI2 in 1/3-octave bands through the low frequency model.



(10.d) SRI3 in 1/3-octave bands for the low, medium and high frequency models

Figure 10

ing to the experimental data and the simulations as:

$$p^2_{exp} = \beta p^2_{num} \rightarrow SPL_{exp} = SPL_{num} + C \qquad (1)$$

where the variables with the exp subscript are those measured during lift-off, the variables with the num subscript are obtained with the numerical model and the adaptation term is $C = 10 \log \beta$.

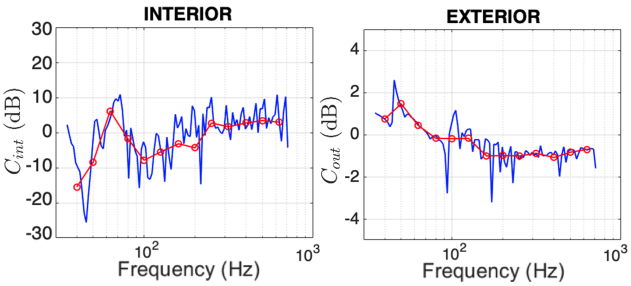


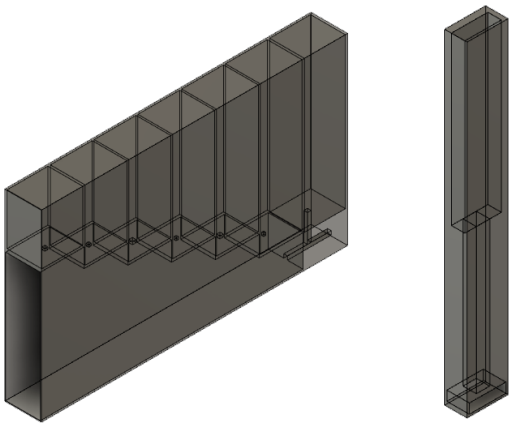
Figure 11: Adaption terms by 1/24-octave (blue) and 1/3-octave (red) bands.

C is obtained for both the acoustic field inside (C_{int}) and outside (C_{out}) the fairing. Figure 11 shows the results for C_{int} and C_{out}. It can be observed that C_{int} is greater than C_{out} since it includes all the discrepancies between the fairing structures.

The mean value of the sound pressure level inside and outside the fairing is presented to show the consistency in both structural and acoustic response between the different frequency ranges. Moreover, to assess the performance of the modelling framework, numerical results are compared with the experimental results available. Figure 10.a left shows the comparison between the measured mean SPL of the internal microphones; the mean of the surface pressure at the two corresponding locations in the FEM/BEM model and an estimation of the surface pressure for the hybrid and SEA models, considering that the surface pressure is the mean SPL of the cavity plus 3 dB due to the reflection of the sound field on the wall surface. Regarding the continuity between models, a very good agreement is found between the two primary models, FEM/BEM and SEA, with differences lower than 1 dB on the overlapping bands. The difference between these models and the secondary hybrid model is larger up to 6 dB. Figure 10.a right presents the mean SPL outside the VEGA fairing. For the test, this corresponds to the mean of the two microphones on the external face. For the FEM/BEM model this magnitude is calculated averaging the surface pressure at the two corresponding locations in the numerical model. For the hybrid and SEA models, this value is fixed and associated to the Diffuse Acoustic Field. Therefore, there is not any difference between the results of these latter models and the test. Differences between the test and the FEM/BEM model are lower than 1 dB. Although there are noticeable differences between the test measurements and the numerical models, especially for the low frequency bands, these are considered acceptable. Therefore, the modelling framework proposed is considered valid for the analysis of the vibro-acoustic response of a VEGA-like fairing designed.

In order to evaluate the performance of the fairing analysed as acoustic protection of the launch vehicle payload, three sound reduction indices have been defined. Figure 10.b shows the first sound reduction index (SRI1) based on the difference between 6 external SPL and 2 internal SPL. The second sound reduction index, shown in Figure 10.c, evaluates the mean of point transmission loss determined from the interior and exterior surface pressures at eight locations. The transmission loss at each location and the mean value show a noticeable dispersion. Finally, the mean transmission loss (SRI3) determined as the level difference between the mean SPL on the outer face of the fairing wall and the mean SPL inside it is shown in Figure 10.d. Both low and high frequency models show good agreement in the overlapping bands. The maximum difference is of around 1 dB even if the first 1/3-octave band shown for the SEA model is not inside its considered applicability range.

4. CONCEPT DESIGN FOR NOISE REDUCTION



(12.a) Launch pad unit cell. (12.b) Fairing unit cell.

Figure 12: 3D view of the proposed structure.

The acoustic metamaterials that we develop consist of panels made of periodic distributions of waveguides loaded by Helmholtz resonators. More information regarding the concepts to understand the physical mechanisms producing the perfect absorption of sound and the low transmission through the structures developed can be found in [4] [30] [6] [5] [31].

The transmission loss of the existing fairing has been analysed by means of the data provided by ESA. The transmission loss (TL) presents a deep around 400 Hz. Therefore, we develop solutions that will improve this TL and will introduce additional effects like acoustic absorption in the problematic bands of frequencies. In particular, the solution proposed in the launch pad is based on increasing the absorption capabilities, in such a way that the reflected wave through the rocket will be strongly reduced in the range of frequencies of interest between 125 and 500 Hz. Then, the solution proposed for the fairing will reduce the transmission loss from 250 Hz introducing absorption peaks around 400 Hz to avoid the problematic range of frequencies.

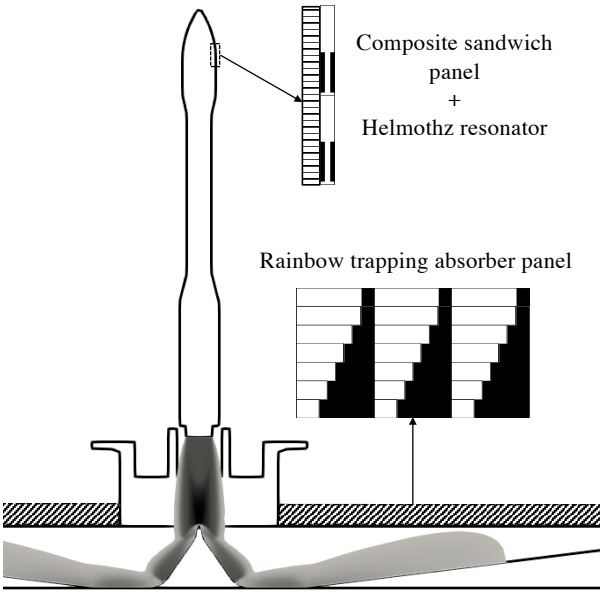
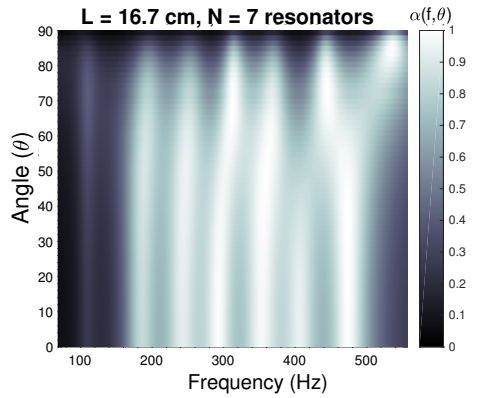


Figure 13: Sketch of the implementation of both solutions in the VEGA launch pad. Rainbow trapping absorber implemented as a cover of the exhaust ducts and the metamaterial added to the existing wall at the fairing.

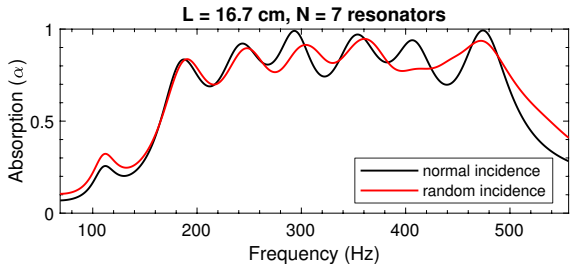
4.1. Noise reduction metamaterials for the launch pad

The ground base usually includes sub-surface channels the design of which is mostly oriented to act on exhaust gases. The channel walls and bottom, mainly made with refractory concrete, are highly reflecting for sound waves, and therefore far to be optimal from the noise management point of view [2, 32]. The two main methods to reduce the noise pressure levels are sound absorption, mainly by water injection, and the control of sound reflection, by acting on the shape of flame deflectors and coverings. The strategy proposed is to design a structure which is able to act on the two current basic mechanisms for sound control, by covering the channels with a highly absorbing structure. The goal is to design a panel that decreases sound levels present at the launch pad area, and consequently, reduce the reflection of the acoustic load back to the fairing. The panel is to be placed on the ground, partially covering the exhaust gas channels. To achieve the desired dimensions, the panel will be composed by the periodic repetition of a unit cell which be seen on Figure 12.a. The unit cell consists in a sequence of Helmholtz resonators with different geometries, whose geometrical parameters are carefully calculated by optimisation methods to achieve a high absorption in a frequency band that runs from 125 to 500 Hz. The optimal solution has 9 resonators and a length of 32.85 cm as can

be seen on [5]. The resulting structure has been called a rainbow trapping absorber, because sound is trapped and dissipated withing the structure at different depths, depending on its frequency.



(14.a) Map angle of incidence versus frequency of the absorption coefficient.



(14.b) Comparison of the absorption coefficient for the diffuse field incidence with the absorption at normal incidence.

It is important to keep in mind that the acoustic panel will be composed of a large number of unit cells. A single cell is very light, but the total weight of the structure may increase considerably for a large number of cells. Therefore, a trade-off of the absorption with the number of resonators has been done to reach a compromise solution between the total area and the weight of the structure. Different panel depths (L) from 5 to 40 cm and different number of resonators (N) from 2 to 10 have been studied. Except for a very small number of resonators or very small thickness, the peaks of absorption are high and reach the perfect absorption in the configuration. The final geometry has half the width and fewer resonators than the optimal structure. Figure 12.a shows the structure that has 7 resonators and 16.7 cm of length. As can be seen on Figure 14.b, the metamaterial structure does not have a flat absorption band but presents high peaks of absorption and a mean absorption of 0.78.

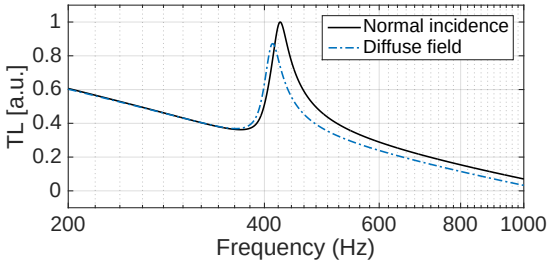
The configuration proposed has been optimised with a normal incident plane wave as an excitation. However, if other angles of incidence are considered the sound absorption of the structure will change. This is an important topic, because as it has been seen on Section 3.1, the flow field in exhaust channels does not have a main direction in that region. Thus, the influence of oblique incidence has been analysed. The absorption coefficient has been calculated as a function of frequency and the angle of incidence. Figure 14.a shows that the absorption coefficient remains almost constant up to angles of incidence of 60°. Furthermore, the absorption coefficient has been calculated for a diffuse acoustic incidence. Figure 14.b compares the absorption for a diffuse field incidence and for normal incidence. As the absorption coefficient for angles bigger than 60° is reduced, the perfect absorption behaviour is also reduced for the diffuse incident field. However, the diffuse field curves of the panel do not change much since the cosine function does not decrease too much until about 60°. Hence, the structure even at oblique incidence presents a good behaviour.

4.2. Noise reduction metamaterials for the fairing

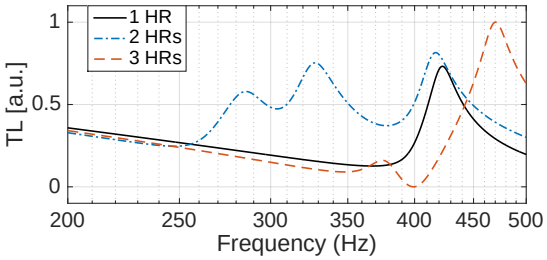
In this configuration, the panel is introduced behind the existing fairing wall as can be seen on Figure 13. This structure is asymmetric and therefore, the scattering response will be different on each side of the structure. On the one hand, when the incidence wave comes from outside the fairing, the sound reflection, R^+, by the fairing wall is very high due to the high impedance of the composite. As a consequence, the sound transmission, T^+ is expected to be low. Due to these properties, the absorption effect added by the panel of Helmholtz resonators is expected to be limited, but will contribute to improve the transmission loss of the reference panel. On the other hand, when the incident wave corresponds to a wave coming from inside the fairing, the composite wall act almost as a rigid wall and the problem can be controlled by the reflection coefficient R^-. Therefore, this solution is expected to improve both the transmission loss as well as the absorption of the system.

The fairing structure considered here is a sandwich panel made of two walls of M55J composite material and an aluminium honeycomb structure inbetween. The geometry and the material properties of the structure are the same as in Section 3.2. The scattering properties of the complete system will depend on the geometrical parameters. Therefore, an optimisation method, in which the geometrical parameters of the structure are tuned to obtain the desired transmission and absorption, has been developed. The number of resonators along the panel thickness is fixed to a single resonator, which is the best configuration in terms of mass reduction and improvement of TL as well as absorption. Besides, the thickness of the panel has been fixed to 1 cm, allowing a thin panel that could be easily glued to the fairing wall. The optimisation is achieved for an incident plane wave coming from inside the fairing and considering both normal incidence and diffuse field. The unit cell obtained can be seen on Figure 12.b. The Transmission Loss (TL) for both conditions are depicted in Figure 15.a. The results for the optimisation with normal incidence present an average TL of 140 dB with a peak of 167 dB at 411 Hz. While the results in diffuse field condition present an average TL of 142 dB with a peak of 174 dB at 423 Hz. From the

results, it is clear that the behaviour is mainly the same.



(15.a) Transmission Loss optimised in normal incidence and diffuse field conditions.



(15.b) TL of optimised with 1, 2 and 3 HRs.

As the optimised structure is composed of only one resonator along the thickness, there is in only one peak of absorption at 400 Hz. But as in the case of the launch pad solution, increasing the number of resonators will widen the frequency band of absorption. Figure 15.b illustrates the TL for different number of resonators. The configuration with 2 Helmholtz resonators produces 2 peaks of absorption, while the configuration with 3 Helmholtz resonators produces 3 peaks. Despite a better TL, it has to be noted that the thickness of the treatment increases with the number of resonator and this will impact directly the mass of the applied treatment. The area density of the panel is therefore doubled in the case of 2 HRs and tripled in the case of 3 HRs. Hence, the solution with one resonator is optimal because it provides perfect absorption and moreover minimises the mass added to the fairing.

5. CONCLUSIONS

In the context of the design of a noise reduction technique to improve the sound attenuation during space vehicles launch, a numerical modelling framework has been defined. Computational fluid dynamics has been used to obtain information about the phenomena that occur at launch, facilitating the comprehension of the generation and propagation mechanisms of noise. Through Schlieren images the shock waves have been identified. By displaying the Sound Pressure Level for different instants, it has been found that the SPL maxima appear due to the normal shock wave generated by the jet and its impingement with the deflector. Moreover, the propagation of the upstream sound waves and the vertical directivity of the pressure over the fairing have been observed.

For the vibro-acoustic problem, a numerical model composed of a set of numerical models for different frequency ranges have been proposed. It is composed of two main models, a discretised model based on FEM and BEM for the low frequency range and a SEA model for the high frequency range. The models developed show a good frequency consistency, showing in general good agreement in the overlapping frequency bands. Also, there is good agreement between models and the test on the outer surface pressure. While for the internal surface pressure noticeable differences are shown. Nevertheless, given the limited information known and the important hypothesis done, the results are considered adequate for the aim that is to provide of a modelling framework and a reference case for subsequent work packages.

On the acoustic domain, two metamaterial structures made of arrangements of Helmholtz resonators have been developed as noise mitigation systems for the launch pad and the fairing. In the case of the launch pad, the structure will be placed in the top of the exhaust channels. After a trade-off analysis of the absorption with the number of resonators, the final configuration is composed of 7 resonators and therefore has a wide frequency band of maximum absorption between 200 and 500 Hz. In the case of the fairing, the metamaterial is added to the existing wall. As the mass is critical for the fairing, the metamaterial consist only of one resonator. Therefore the solution introduce only an absorption peak around 400 Hz. Experimental validation of the proposed mitigation will be performed in the next phase of the study.

ACKNOWLEDGMENTS

Authors acknowledge the support of the European Space Agency under contract 4000126316/19/NL/LvH of project REDLAUCH: Launch Sound Level Reduction. The work was supported by Spanish Ministry of Science and Innovation through project DIN2019-010877, project RTI2018-102256-B-100 of Mineco/FEDER and project PID2019-109175GB-C22. The authors very much appreciate the support offered by ESI Group.

REFERENCES

[1] K. M. Eldred. Acoustic loads generated by the propulsion system. Technical report, NASA Technical Reports Server, 1971.

[2] Chongwen Jiang, Tianyixing Han, Zhenxun Gao, and Chun-Hian Lee. A review of impinging jets during rocket launching. *Progress in Aerospace Sciences*, 109:100547, aug 2019.

[3] Jorge P Arenas and Ravi N Margasahayam. NOISE AND VIBRATION OF SPACECRAFT STRUCTURES. *Ingeniare. Revista chilena de ingeniería*, 14(3), dec 2006.

[4] N. Jiménez, W. Huang, V. Romero-García, V. Pagneux, and J.-P. Groby. Ultra-thin metamaterial

for perfect and quasi-omnidirectional sound absorption. *Applied Physics Letters*, 109(12), sep 2016.

[5] Noé Jiménez, Vicent Romero-García, Vincent Pagneux, and Jean-Philippe Groby. Rainbow-trapping absorbers: Broadband, perfect and asymmetric sound absorption by subwavelength panels for transmission problems. *Scientific Reports*, 7(1), oct 2017.

[6] V. Romero-García, G. Theocharis, O. Richoux, A. Merkel, V. Tournat, and V. Pagneux. Perfect and broadband acoustic absorption by critically coupled sub-wavelength resonators. *Scientific Reports*, 6(1), jan 2016.

[7] R Picó, I Herrero-Durá, V Sánchez-Morcillo, LJ Salmerón-Contreras, and LM Garcia-Raffi. Acoustic behavior of the vega launch pad environment. *Proceedings of EuroRegio*, 2016.

[8] T Nonomura, H Nakano, Y Ozawa, D Terakado, M Yamamoto, K Fujii, and A Oyama. Large eddy simulation of acoustic waves generated from a hot supersonic jet. *Shock Waves*, 29(8), 2019.

[9] Christopher KW Tam. Supersonic jet noise. *Annual review of fluid mechanics*, 27(1):17–43, 1995.

[10] Max Kandula. Broadband shock noise reduction in turbulent jets by water injection. *Applied Acoustics*, 70(7):1009–1014, jul 2009.

[11] Daniel Allgood, Grady Saunders, and Lester Langford. Reduction of altitude diffuser jet noise using water injection. In *50th AIAA Aerospace Sciences Meeting including the New Horizons Forum and Aerospace Exposition*, jan 2012.

[12] L.M. Garcia-Raffi, L.J. Salmerón-Contreras, I. Herrero-Durá, R. Picó, J. Redondo, V.J. Sánchez-Morcillo, K. Staliunas, N.J.E. Adkins, A. Cebrecos, N. Jiménez, and V. Romero-García. Broadband reduction of the specular reflections by using sonic crystals: A proof of concept for noise mitigation in aerospace applications. *Aerospace Science and Technology*, 73:300–308, feb 2018.

[13] Denis Gély, Georges Elias, Flavia Mascanzoni, and Henri Foulon. Acoustic environment of the vega launch vehicle at lift-off. In *Proceedings of the Forum Acusticum, Budapest*, 2005.

[14] Seiji Tsutsumi, Susumu Kato, Kota Fukuda, Ryoji Takaki, and Kyoichi Ui. Effect of deflector shape on acoustic field of launch vehicle at lift-off. In *47th AIAA Aerospace Sciences Meeting including The New Horizons Forum and Aerospace Exposition*, jan 2009.

[15] Jorge P Arenas and Malcolm J Crocker. Recent trends in porous sound-absorbing materials. *Sound & vibration*, 44(7):12–18, 2010.

[16] Dah-You Maa. Potential of microperforated panel absorber. *the Journal of the Acoustical Society of America*, 104(5):2861–2866, 1998.

[17] H. Fuchs and Xueqin Zha. Micro-perforated structures as sound absorbers : A review and outlook. *Acta Acustica United With Acustica*, 92:139–146, 2006.

[18] Pedro Cobo and Francisco Simón. Multiple-layer microperforated panels as sound absorbers in buildings: a review. *Buildings*, 9(2):53, 2019.

[19] Jinkyo Lee and George Warner Swenson. Compact sound absorbers for low frequencies. *Noise Control Engineering Journal*, 38(3):109–117, 1992.

[20] DH Lee and YP Kwon. Estimation of the absorption performance of multiple layer perforated panel systems by transfer matrix method. *Journal of sound and vibration*, 278(4-5):847–860, 2004.

[21] Pedro Cobo, Heidi Ruiz, and Julián Alvarez. Double-layer microperforated panel/porous absorber as liner for anechoic closing of the test section in wind tunnels. *Acta Acustica united with Acustica*, 96(5):914–922, 2010.

[22] Zhengqing Liu, Jiaxing Zhan, Mohammad Fard, and John Laurence Davy. Acoustic properties of multilayer sound absorbers with a 3d printed microperforated panel. *Applied Acoustics*, 121, 2017.

[23] Yonghua Wang, Chengchun Zhang, Luquan Ren, Mohamed Ichchou, Marie-Annick Galland, and Olivier Bareille. Sound absorption of a new bionic multi-layer absorber. *Composite Structures*, 108:400–408, 2014.

[24] Michael James Lighthill. On sound generated aerodynamically i. general theory. *Proceedings of the Royal Society of London. Series A. Mathematical and Physical Sciences*, 211, 1952.

[25] Mara S. Escarti-Guillem, Sergio Hoyas, and Luis M. García-Raffi. Rocket plume URANS simulation using OpenFOAM. *Results in Engineering*, 4:100056, dec 2019.

[26] ECSS Secretariat. Spacecraft mechanical loads analysis handbook. *European Cooperation for Space Standardization*, 2013.

[27] Phil J Shorter and Robin S Langley. Vibro-acoustic analysis of complex systems. *Journal of Sound and Vibration*, 288(3):669–699, 2005.

[28] E Roibás, M Chimeno, J López-Díez, and F Simón. A mode count procedure for mid-frequency analysis of complex vibro-acoustic systems. *Aerospace Science and Technology*, 29, 2013.

[29] ESI Group. *VAOne 2018 Users Guide*, 2018.

[30] V. Romero-García, G. Theocharis, O. Richoux, and V. Pagneux. Use of complex frequency plane to design broadband and sub-wavelength absorbers. *The Journal of the Acoustical Society of America*, 139(6), jun 2016.

[31] Iván Herrero-Durá, Alejandro Cebrecos, Rubén Picó, Vicente Romero-García, Luis Miguel García-Raffi, and Víctor José Sánchez-Morcillo. Sound absorption and diffusion by 2d arrays of helmholtz resonators. *Applied Sciences*, 10(5), mar 2020.

[32] G. Dumnov, D. Mel'nikov, and V. Komarov. Acoustic loads on rockets during launch. In *36th AIAA/ASME/SAE/ASEE Joint Propulsion Conference and Exhibit*, jul 2000.